

Simulation study on lead-free double Cs₂AgBiBr₆/GaAs tandem solar cells

M. J. Yu, J. R. Yuan ^{*}, X. H. Deng

*School of Physics and Materials Science, Nanchang University, Nanchang
330031, China*

Cs₂AgBiBr₆, a double perovskite devoid of lead, is a remarkable alternative to traditional perovskite solar cells. This research utilised Silvaco TCAD simulation software to construct and examine lead-free double Cs₂AgBiBr₆/gallium arsenide tandem devices. By optimising the perovskite layer thickness, the thickness and doping concentration of the gallium arsenide base layer, selecting an appropriate carrier transport layer thickness, and integrating an anti-reflective layer, the conversion efficiencies of the four-terminal lead-free double Cs₂AgBiBr₆/gallium arsenide tandem solar cell is achieved up to 31.71%. Based on the study of 4-T tandem devices, current matching of 2-T tandem devices was performed. The 2-T tandem device achieved an energy conversion efficiency of 26.35% by optimising the doping concentration of the GaAs substrate layer. Furthermore, the 2-T tandem device energy conversion efficiency remains at 23.40% following the current matching under spectral AM0, which has the potential application in space.

(Received November 2, 2024; Accepted January 6, 2025)

Keywords: Cs₂AgBiBr₆/GaAs tandem solar cells, Lead-free double perovskite,
Gallium arsenide, Silvaco TCAD

1. Introduction

Perovskite has attracted considerable attention and scholarly investigation owing to its unique photovoltaic characteristics, which encompass powerful light absorption, extended carrier diffusion length and lifetime, tunable bandgap, and cost-effectiveness [1-6]. Xu Jixian and his team [7] at the USTC recently established a certified world record-breaking steady-state efficiency of 26.7% for a perovskite cell. Nevertheless, the organic-inorganic halide lead-based perovskite material is detrimental to the environment and the human body due to its contents of lead and the organic ions (MA⁺ and FA⁺), which are susceptible to self-degradation in the absence of external interference [8-10]. The double perovskite structure A₂B'B''X₆ has been suggested as a promising candidate for non-toxic, stable, and highly efficient perovskite materials. This structure replaces the two toxic lead ions in traditional lead-based perovskites with a pair of heterovalent metal cations. This approach is intended to address the toxicity and stability issues. Scholars have successfully synthesised several double perovskite materials, such as Cs₂NaBiI₆ [11], Cs₂AgInCl₆ [12], Cs₂AgBiX₆ (X=I, Cl, Br) [13-14], and Cu₂AgBiI₆ [15]. The properties of Pb-based halide perovskite

* Corresponding author: yuanjiren@ncu.edu.cn

<https://doi.org/10.15251/JOR.2025.211.1>

are most closely resembled by $\text{Cs}_2\text{AgBiBr}_6$, which has the most potential for application among these materials.

The presence of the shockley–queisser limit constrains the performance of solar cells [16]. Tandem devices, generally comprising two subcells, can break the shockley-queisser limit and hence enhance performance [17-18]. The top cell of a tandem device features a wider bandgap to capture the shorter wavelength segment of sunlight, and the bottom cell is absorbed with the lengthy wavelength part, thereby reducing unnecessary energy loss. The top cell of a tandem device possesses a broader bandgap to capture the shorter wavelength segment of sunlight, while the bottom cell is designed for the longer wavelength segment, hence minimising unnecessary energy loss [19-20]. Tandem devices are often classified into four-terminal and two-terminal categories. The 4-T tandem device comprises two independent subcells, which are only optically related. The 2-T tandem device consists of two subcells linked by intermediate layers. The one with the lower current in the subcells determines the current of the two-terminal tandem device. Thus, current matching is essential for developing the high energy conversion efficiency 2-T tandem device [21].

Researchers have recently synthesised tandem structures of perovskite with GaAs, perovskite, CIGS, and crystalline silicon based on theoretical guidance [22-26]. Cardinaletti et al [27] illustrate the feasibility of applying perovskite solar cells for space. Nevertheless, the application of conventional perovskite solar cells in space is restricted by the presence of organic ions that are readily decomposed. Park and his colleagues [28] investigated perovskite/gallium arsenide tandem devices with photovoltaic conversion efficiencies of 24.27% for 2-T devices and 25.19% for 4-T devices. Kurtz's model [29] indicates that utilising GaAs as the bottom cell in the tandem device, which keeps the top cell's band gap from 1.90 to 2.10 eV, is optimal. The material of $\text{Cs}_2\text{AgBiBr}_6$ is non-toxic and has superior thermal stability. Still, its bandgap is also suitable for use as a top cell and has the potential for space applications [30-34].

In this paper, a theoretical analysis and study of lead-free double $\text{Cs}_2\text{AgBiBr}_6$ /gallium arsenide tandem solar cells, including 4-T and 2T lead-free double $\text{Cs}_2\text{AgBiBr}_6$ /gallium arsenide tandem devices, are conducted. To mitigate parasitic losses and reflection losses, the thicknesses of the GaAs substrate, the carrier transport layer, and the $\text{Cs}_2\text{AgBiBr}_6$ were optimised. An anti-reflective layer with excellent performance is implemented to obtain higher performance in 4-T tandem devices, and the impact of ITO layer thickness on the performance for the lighted side of tandem devices is examined. Subsequently, the 2-T tandem devices were currently matched, and the impact of the GaAs substrate layer doping concentration on the performance of tandem devices was examined. The 2-T $\text{Cs}_2\text{AgBiBr}_6$ /gallium arsenide tandem device obtains an efficiency of 26.35% and maintains an energy conversion efficiency of 23.40% in the AM0 spectrum. The 4-T $\text{Cs}_2\text{AgBiBr}_6$ /gallium arsenide tandem device achieves a high energy conversion efficiency of 31.71%.

2. Device structure and simulation parameters

The atlas module of silvaco tcad simulation software will be employed in this paper to simulate the solar cell and the tandem device to achieve the best possible performance. The theoretical foundation for the atlas simulation of the perovskite solar cell comprises three essential equations: the Poisson equation (Formula (1)), the continuity equation (Formula (2)), and the drift-

diffusion equation (Formula (3)) [35]. Newton's and maxtraps methods are employed to resolve the convergence issue. This paper's simulation also considers the Shockley-Read-Hall (SRH) composite model, Auger composite model, Band-to-Band composite model, and the effects of tunnelling on the performance of the device [36-38]. The default illumination conditions are AM1.5G, 1000mW/cm², and 300K temperature.

Fig. 1 illustrates the configuration of ITO/ZnO/Cs₂AgBiBr₆/MoO₃/ITO used as the top cell, and high-efficiency GaAs bottom cell were designed by Bertness et al [39] and Park et al [33]. A 10nm vacuum layer is inserted between the subcells in the four-terminal Cs₂AgBiBr₆/gallium arsenide tandem device, whereas a 10 nm ITO tunnelling layer connects the two subcells in the two-terminal Cs₂AgBiBr₆/gallium arsenide tandem device. Table 1 and Table 2 contains the material parameters that were implemented during the simulation. The software's internal files can be used to directly access the nk parameters of the electrode materials and a portion of the conventional semiconductor materials [40]. The remaining optical parameters of nk are derived from the literature [41-46], and the electrical data used in the simulation of this paper are also derived from the literature [47-51].

$$\frac{\partial^2 \phi}{\partial x^2} = \frac{q}{\epsilon} (n - p) \quad (1)$$

$$\frac{\partial n}{\partial t} = \frac{1}{q} \frac{\partial J_n}{\partial x} + G - R \quad \frac{\partial p}{\partial t} = -\frac{1}{q} \frac{\partial J_p}{\partial x} + G - R \quad (2)$$

$$J_n = qD_n \frac{\partial n}{\partial x} - q\mu_n n \frac{\partial \phi}{\partial x} \quad J_p = -qD_p \frac{\partial p}{\partial x} - q\mu_p p \frac{\partial \phi}{\partial x} \quad (3)$$

Table 1. Parameters of all used materials.

Parameter	ZnO	Cs ₂ AgBiBr ₆	MoO ₃	GaAs	GaInP
N _A (cm ⁻³)	-	10 ¹⁹	10 ¹⁸	10 ¹⁷ (Base)	3×10 ¹⁷ (BSF)
N _D (cm ⁻³)	10 ¹⁸	10 ¹⁹	-	10 ¹⁹ (Emitter)	10 ²⁰ (Window)
E _g (eV)	3.3	2.05	3	1.42	1.61
Aff (eV)	4.1	3.79	2.5	4.07	4.4
ε _r	9	5.80	12.5	13.2	12.1
N _C (cm ⁻³)	2.2×10 ¹⁸	1×10 ²⁰	2.2×10 ¹⁸	4.35×10 ¹⁷	7.18×10 ¹⁷
N _V (cm ⁻³)	1.9×10 ¹⁹	1×10 ²⁰	1.8×10 ¹⁹	8.16×10 ¹⁸	8.87×10 ¹⁸
μ _n (cm ² /(V s))	100	0.37	25	8000	4600
μ _p (cm ² /(V s))	25	0.37	100	400	150
τ _n (s)	2.83×10 ⁻²	1.75×10 ⁻⁸	1×10 ⁻⁷	1×10 ⁻⁹	1
τ _p (s)	2.83×10 ⁻²	1.75×10 ⁻⁸	1×10 ⁻⁷	2×10 ⁻⁸	1

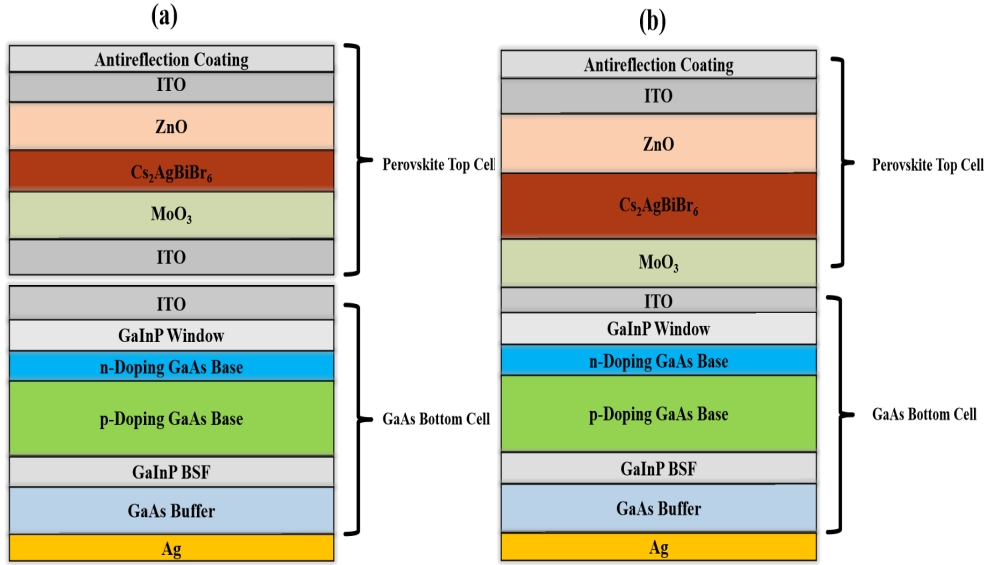


Fig. 1. Lead-free double $\text{Cs}_2\text{AgBiBr}_6/\text{GaAs}$ tandem device (a) four-terminal structure (b) two-terminal structure.

3. Results and discussion

3.1. Simulation and optimisation of four-terminal $\text{Cs}_2\text{AgBiBr}_6/\text{GaAs}$ tandem devices

3.1.1. Thickness study of the absorbing layer in subcells

Initially, the GaAs substrate is set to $3.5 \mu\text{m}$, and the thickness of the $\text{Cs}_2\text{AgBiBr}_6$ is enlarged from $0.1 \mu\text{m}$ to $2 \mu\text{m}$. The efficiency simulation results are illustrated in Fig. 2(a). The energy conversion efficiency of both perovskite $\text{Cs}_2\text{AgBiBr}_6$ and gallium arsenide exhibits a tiny improvement in efficiency with a relatively thin $\text{Cs}_2\text{AgBiBr}_6$ layer, followed by a gradual decrease in efficiency as the thickness increases. The tandem device's total efficiency exhibits the same trend as the subcell's. The spectrum absorption overlap between subcells indicates that an increase in the thickness of the $\text{Cs}_2\text{AgBiBr}_6$ results in a reduction of photons captured by the GaAs cell, hence diminishing the energy conversion efficiency of the latter. Additionally, the increase in the thickness of the $\text{Cs}_2\text{AgBiBr}_6$ will make the carrier diffusion distance longer, which makes the carriers more likely to be compounded in the diffusion process, resulting in a decrease in the J_{sc} , ultimately decreasing the performance of the four-terminal $\text{Cs}_2\text{AgBiBr}_6/\text{gallium arsenide}$ tandem device.

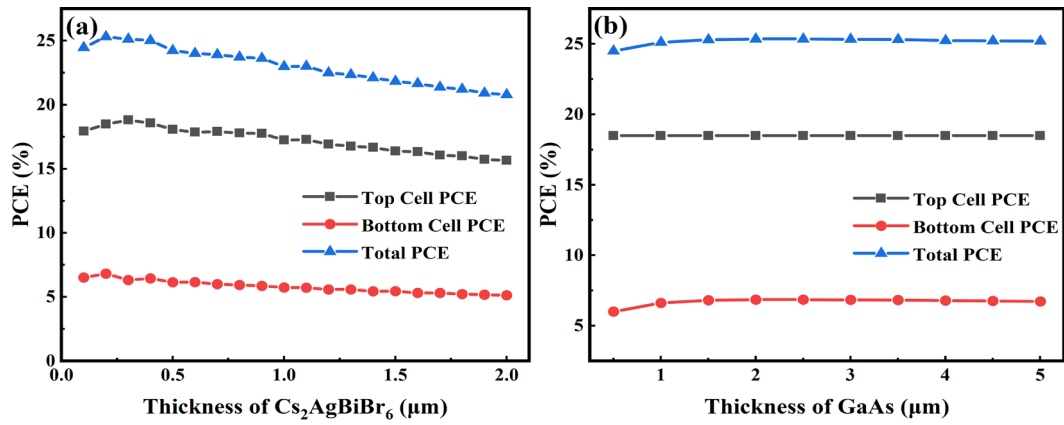


Fig. 2. The energy conversion efficiency of subcells and four-terminal tandem devices varies with the thickness of (a) $\text{Cs}_2\text{AgBiBr}_6$ and (b) gallium arsenide substrate.

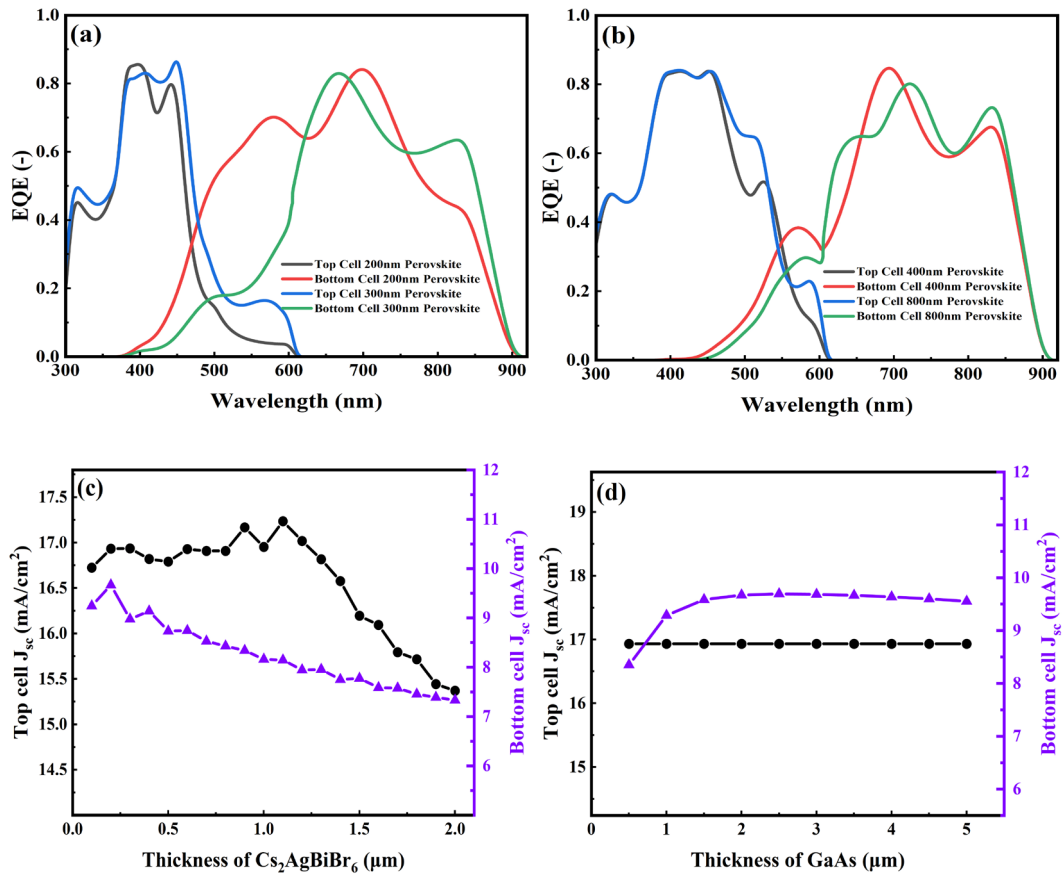


Fig. 3. (a) and (b) are the eqe of subcells with different thicknesses of $\text{Cs}_2\text{AgBiBr}_6$, and the effects of the thickness of $\text{Cs}_2\text{AgBiBr}_6$ and GaAs substrate on the J_{sc} of the subcells are represented by (c) and (d), respectively.

To further explore the reason and mechanism of the change in the photovoltaic conversion efficiency, the J_{sc} and the e_{qe} (external quantum efficiency) are simulated in this paper, respectively. Figs. 3(c) and 3(d) demonstrate that the trends of J_{sc} and energy conversion efficiency are nearly identical as the thickness of both the subcells absorber layers increases, indicating that variations in J_{sc} influence the trend in energy conversion efficiency. Fig. 3(a) illustrates the e_{qe} of the subcells at thicknesses of 200 nm and 300 nm for $Cs_2AgBiBr_6$, revealing an overlap in solar spectrum absorption between the subcells. The dominant absorption spectral wavelength of the $Cs_2AgBiBr_6$ is 300 ~ 600 nm, while the major absorption spectral wavelength of the GaAs cell is 400 ~ 900 nm. Enhancing the thickness of $Cs_2AgBiBr_6$ from 200 nm to 300 nm enhances the e_{qe} of the $Cs_2AgBiBr_6$ cell, whereas the e_{qe} of the GaAs cell drastically declines in the 400 ~ 600 nm region. This signifies an increase in absorption in the $Cs_2AgBiBr_6$ cell, whereas absorption in the GaAs cell has markedly decreased, aligning with the trend observed in the J_{sc} variation depicted in Fig. 3(c). Fig. 3(b) illustrates the e_{qe} of the subcells for $Cs_2AgBiBr_6$ thicknesses of 400 nm and 800 nm correspondingly, the figure illustrates that the top cell achieves saturation in e_{qe} , with the J_{sc} at its peak, and for the bottom cell 400 ~ 600 nm wavelength range decreases. Consequently, to maximize the total light absorption, it is imperative to select an appropriate thickness for the $Cs_2AgBiBr_6$ and minimise the reflective losses of the tandem device.

Additionally, the e_{qe} of the GaAs cell is characterised by a continuous fluctuation in the long-wave range, as evidenced by Figs. 3(a) and 3(b). This phenomenon is due to the inability of $Cs_2AgBiBr_6$ to absorb the portion of the solar spectrum exceeding 600 nm, resulting in multiple internal reflections before the light reaches the GaAs substrate layer. This leads to optical interference, causing variations in the e_{qe} of the GaAs cell.

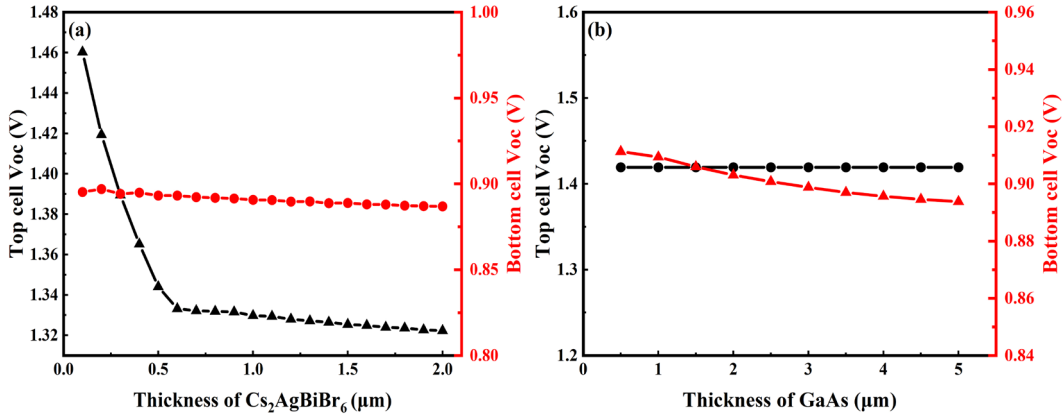


Fig. 4. Variation of subcells V_{oc} with the thickness of (a) $Cs_2AgBiBr_6$ and (b) GaAs substrate.

The thickness of $Cs_2AgBiBr_6$ remains constant at 200 nm, as demonstrated in Fig. 2(b). With a gradual growth in the thickness of the GaAs base, the energy conversion efficiencies of both the bottom cell and the tandem device exhibit a similar trend, gradually increasing and saturating when the GaAs substrate thickness reaches 2.5 μm . Furthermore, the performance of the $Cs_2AgBiBr_6$ cell remains unaffected by variations in the thickness of the absorber layer of the GaAs cell. In summary, the 200 nm $Cs_2AgBiBr_6$ perovskite absorber layer and 2.5 μm GaAs substrate layer are appropriate for the subsequent investigation.

Finally, The V_{oc} of the subcells was investigated as the thicknesses of $\text{Cs}_2\text{AgBiBr}_6$ and the GaAs substrate were augmented. As depicted in Fig. 4, the V_{oc} of the $\text{Cs}_2\text{AgBiBr}_6$ cell markedly diminished when the thickness of $\text{Cs}_2\text{AgBiBr}_6$ expanded from 0.1 μm to 0.5 μm , and a declining trend in V_{oc} was observed as the thickness was further increased from 0.5 μm to 2.0 μm . Modifying the thickness of $\text{Cs}_2\text{AgBiBr}_6$ has a minimal impact on the V_{oc} of the GaAs cell. As the thickness of the gallium arsenide substrate grows, the V_{oc} of the $\text{Cs}_2\text{AgBiBr}_6$ cell remains largely constant. Conversely, the V_{oc} of the GaAs cell progressively diminishes. The standard device's total photoelectric conversion efficiency is 25.35%.

3.1.2. Parasitic absorption losses in carrier transport layers

In tandem solar cells, a significant element influencing the device's light absorption is parasitic absorption. Consequently, it is essential to investigate and enhance the parasitic absorption loss in four-terminal lead-free double perovskite/gallium arsenide tandem devices.

The light absorption of the lead-free double $\text{Cs}_2\text{AgBiBr}_6$ /gallium arsenide tandem solar cell was initially simulated in this work using the top cell carrier transport layer thicknesses of 100 nm ZnO and 150 nm MoO_3 , respectively. As illustrated in Fig. 5(a), the ZnO formed a significant amount of parasitic absorption in the 700~900 nm wavelength spans, significantly impacting the gallium arsenide cell in the 700~900 nm wavelength spans of absorption.

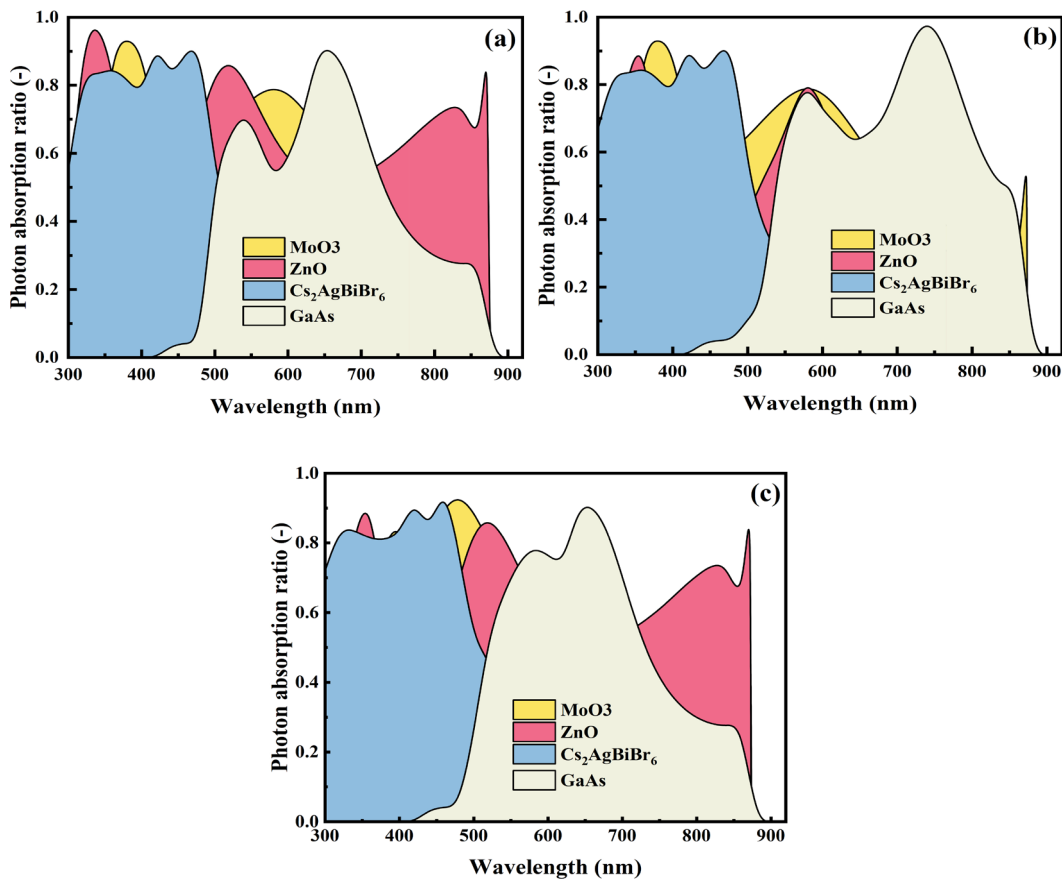


Fig. 5. Photon absorption ratio of MoO_3 , ZnO , $\text{Cs}_2\text{AgBiBr}_6$, and GaAs in four-terminal tandem device with (a) 100 nm ZnO and 150 nm MoO_3 , (b) 20 nm ZnO and 150 nm MoO_3 , (c) 100 nm ZnO and 100 nm MoO_3 .

Additionally, there remains a minor degree of parasitic absorption in other regions of the solar spectrum. Conversely, the hole transport layer of the $\text{Cs}_2\text{AgBiBr}_6$ cell, MoO_3 , demonstrates minimal parasitic absorption within the solar spectrum, leading to a minor impact on the light absorption of the tandem device. Fig. 5(b) illustrates that the parasitic absorption of ZnO in the 700~900 nm wavelength region is markedly enhanced when the ZnO thickness is reduced to 20 nm, resulting in increased optical absorption in the GaAs bottom cell within this wavelength band and diminished parasitic absorption in other wavelength bands. Fig. 5(c) illustrates that the parasitic absorption attributed to MoO_3 diminishes while the thickness of MoO_3 is lowered to 100 nm, hence enhancing the optical absorption of the four-terminal $\text{Cs}_2\text{AgBiBr}_6$ /gallium arsenide tandem device.

The absorption spectra of GaInP in the bottom cell terminate at 600 nm, while ZnO and $\text{Cs}_2\text{AgBiBr}_6$ mostly absorb this portion of the photon in the top cell, resulting in little parasitic absorption loss. In conclusion, the efficiency of tandem devices is significantly influenced by the parasitic absorption caused by the carrier transport layer, and the parasitic absorption losses within the four-terminal $\text{Cs}_2\text{AgBiBr}_6$ /gallium arsenide tandem device can be effectively reduced by selecting an appropriate thickness for the carrier transport layer. This increases the photovoltaic conversion efficiency of a four-terminal lead-free double perovskite $\text{Cs}_2\text{AgBiBr}_6$ /gallium arsenide tandem solar cell from 25.35% to 27.21% in the standard device.

3.1.3. Study of the ARC and the top ITO layer

This study introduces a suitable anti-reflective coating at the top of the 4-T $\text{Cs}_2\text{AgBiBr}_6$ /gallium arsenide tandem device to improve the absorption rate of the tandem device and attain high-performance lead-free double perovskite $\text{Cs}_2\text{AgBiBr}_6$ /gallium arsenide tandem solar cells, and LiF was selected due to its exceptional anti-reflective properties.

Simulations of the performances of both the subcells and tandem were conducted to examine the impact of the LiF anti-reflective layer and its thickness on the tandem device and subcells. Figs 6(a) and 6(b) illustrate the results, which suggest that incorporating the anti-reflective layer enhances the performances of both the tandem device and the subcells. In addition, when the thickness of LiF is gradually increased, the tandem cell and the subcells change the same trend. The photoelectric conversion efficiency initially increases and subsequently declines, with the tandem device achieving peak efficiency at a LiF thickness of 100 nm. This suggests that LiF anti-reflective layers mainly improve light reflection in shorter wavelength bands. Nevertheless, as the LiF thickness exceeds 100 nm, some parasitic absorptions from the anti-reflective layer cause the photoelectric conversion efficiencies of subcells to decrease.

The incorporation of the LiF improves the light absorption of the 4-T $\text{Cs}_2\text{AgBiBr}_6$ /gallium arsenide tandem device in the spans of 300nm~700nm, as demonstrated in Fig. 6(c). This suggests that LiF anti-reflective layers mainly improve light reflection in shorter wavelength bands. Furthermore, as illustrated in Fig. 6(c), reducing the ITO electrode thickness from 100 nm to 20 nm results in an increase in light absorption within the short wavelength range and a decrease in the longer wavelength range; however, the overall light absorption of the device rises, indicating that the reduction in ITO thickness enhances the performance of the 4-T $\text{Cs}_2\text{AgBiBr}_6$ /gallium arsenide tandem device. Fig. 6(d) illustrates that the overall performance declines as ITO thickness grows, suggesting that smaller ITO electrodes enhance the performance of four-terminal $\text{Cs}_2\text{AgBiBr}_6$ /gallium arsenide tandem devices.

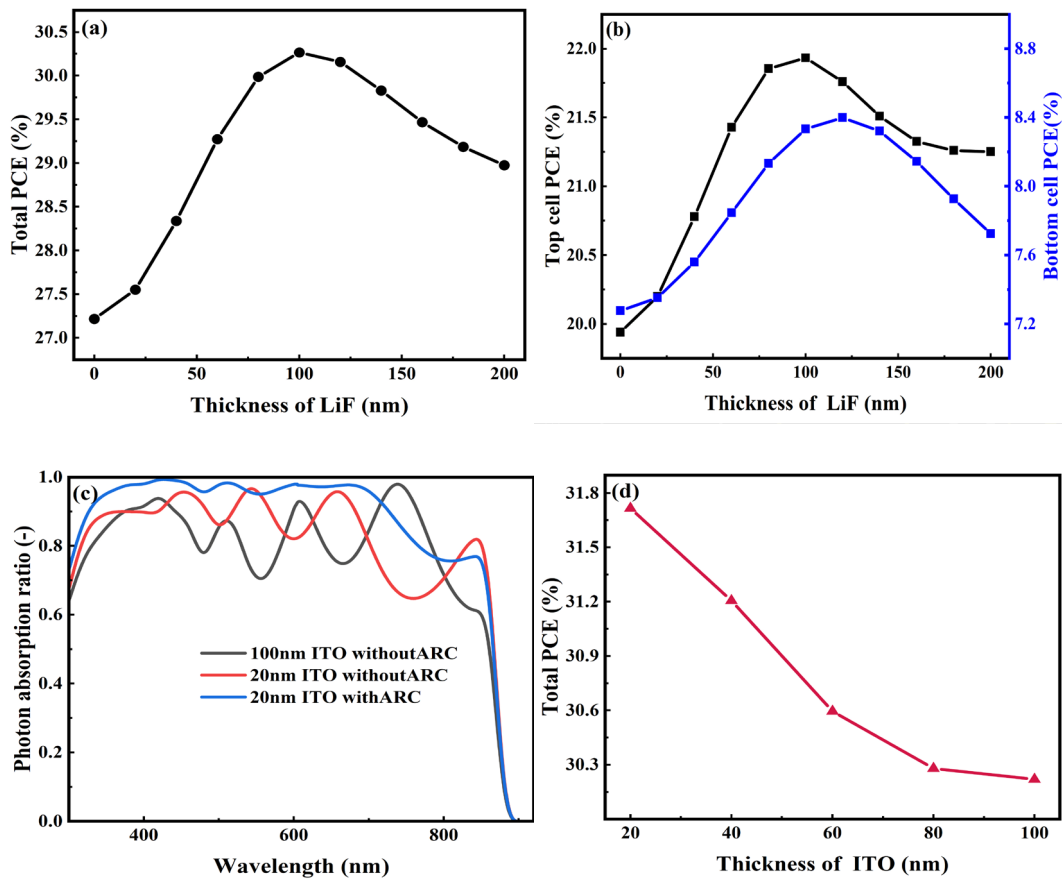


Fig. 6. 4-T tandem devices (a) total photovoltaic conversion efficiency, (b) variation of subcells photovoltaic conversion efficiency with the thickness of LiF, (c) light absorptivity of tandem devices under different conditions, and (d) variation of total photoelectric conversion efficiency of four-terminal tandem devices with the thickness of top ITO electrode.

The photovoltaic conversion efficiency of the 4-T $\text{Cs}_2\text{AgBiBr}_6/\text{gallium arsenide}$ tandem device improved from 27.21% to 31.71% with the incorporation of a LiF antireflection layer atop the device and the optimisation of the top ITO electrode's thickness.

3.1.4. Study of the GaAs substrate layers

The efficiency of gallium arsenide cells is generally substantially affected by the doping concentration of the gallium arsenide substrate layer. The efficiency of the gallium arsenide cell first improves and then gradually declines when the concentration of the gallium arsenide substrate rises. The highest efficiency is achieved at a doping concentration of 10^{17} cm^{-3} , as illustrated in Fig. 7(b). The augmentation of GaAs substrate concentration results in a persistent drop in the J_{sc} of the GaAs cell, as depicted in Fig. 7(a); this causes the V_{oc} to initially improve and then saturate at a doping concentration of 10^{20} cm^{-3} . An increase in doping concentration generates a significant number of composite centres within the GaAs cell; this leads to a substantial rise of the carrier complexation chance in GaAs, and ultimately, this results in a continuous reduction in the device current. Fig. 7(c) illustrates that the energy band bending degree of the GaAs base layer increases as the concentration

of GaAs base doping increases. This results in a more effective extraction of the non-equilibrium carriers generated by the GaAs base layer at the boundary, enhancing the device's V_{oc} to a degree. And, as the energy band approaches its maximum curvature, the V_{oc} of the GaAs cell becomes saturated. Thus, a compromise is made between the V_{oc} and J_{sc} to optimise the performance of the GaAs cell.

According to this research, the doping concentration of the GaAs substrate layer is selected at 10^{17} cm^{-3} . Ultimately, the optimisation resulted in a 31.71% total photoelectric conversion efficiency for the 4-T $\text{Cs}_2\text{AgBiBr}_6/\text{gallium arsenide}$ tandem device.

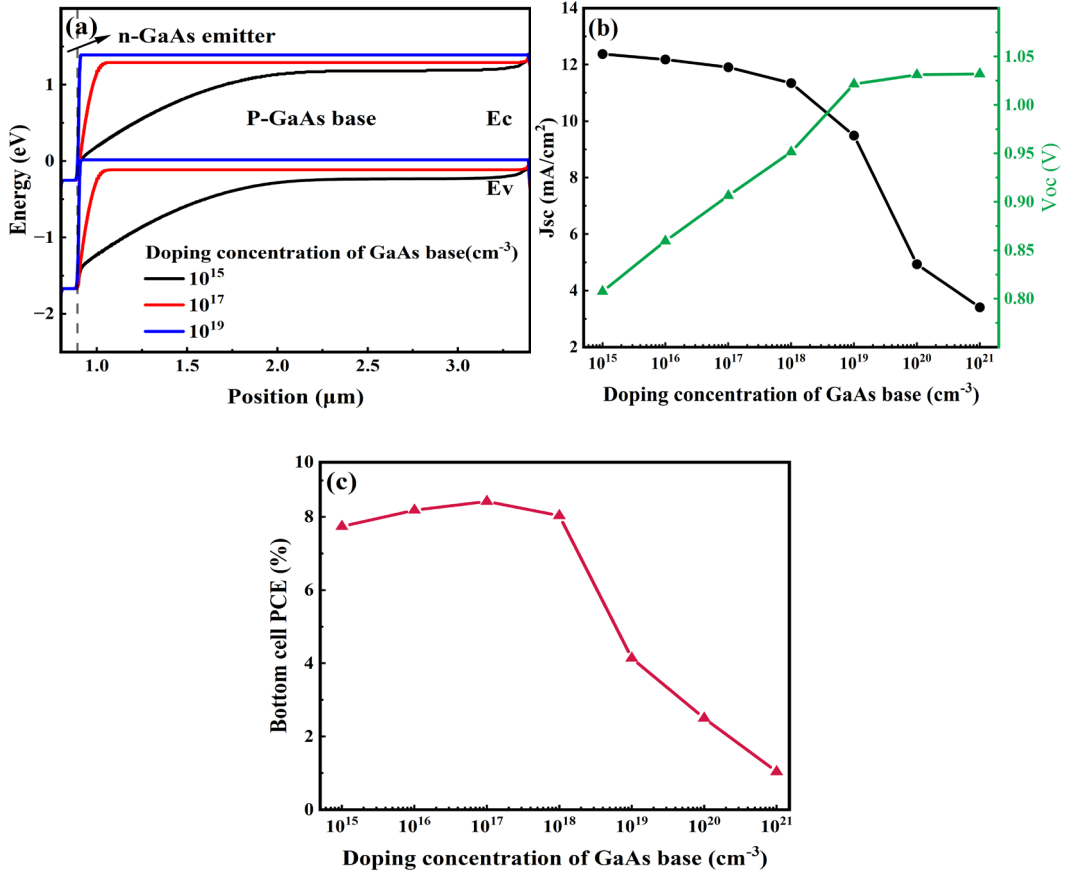


Fig. 7. Variation of (a) J_{sc} and V_{oc} , (b) photovoltaic conversion efficiency, and (c) energy band diagram with doping concentration of GaAs substrate.

3.2. Simulation and optimisation of 2-T $\text{Cs}_2\text{AgBiBr}_6/\text{GaAs}$ tandem devices

The subcells in a four-terminal $\text{Cs}_2\text{AgBiBr}_6/\text{gallium arsenide}$ tandem device exist independently and are only optically related. An intermediate tunnelling layer for two-terminal $\text{Cs}_2\text{AgBiBr}_6/\text{gallium arsenide}$ tandem devices connects the two subcells. Accordingly, the lower current of the subcells will constrain the current of the two-terminal $\text{Cs}_2\text{AgBiBr}_6/\text{gallium arsenide}$ tandem device. Consequently, the current matching is of paramount importance in the design of two-terminal tandem devices. Furthermore, 2-T tandem devices are less expensive than four-terminal

tandem devices, so they have a higher commercial value. Figs. 8(a) and 8(b) illustrate that an increase in the thickness of $\text{Cs}_2\text{AgBiBr}_6$ results in enhanced photon absorption, elevating the current of the $\text{Cs}_2\text{AgBiBr}_6$ cell. The GaAs cells absorb relatively fewer photons within the overlapping wavelengths of the subcell's light absorption; consequently, the bottom cell current decreases. Nonetheless, as the thickness continues to grow, the current of the $\text{Cs}_2\text{AgBiBr}_6$ cell will diminish. The captured photons increase in proportion to the thickness of the GaAs substrate layer, which in turn increases the J_{sc} of the GaAs subcell. But when the thickness continues to augment, the current reaches saturation.

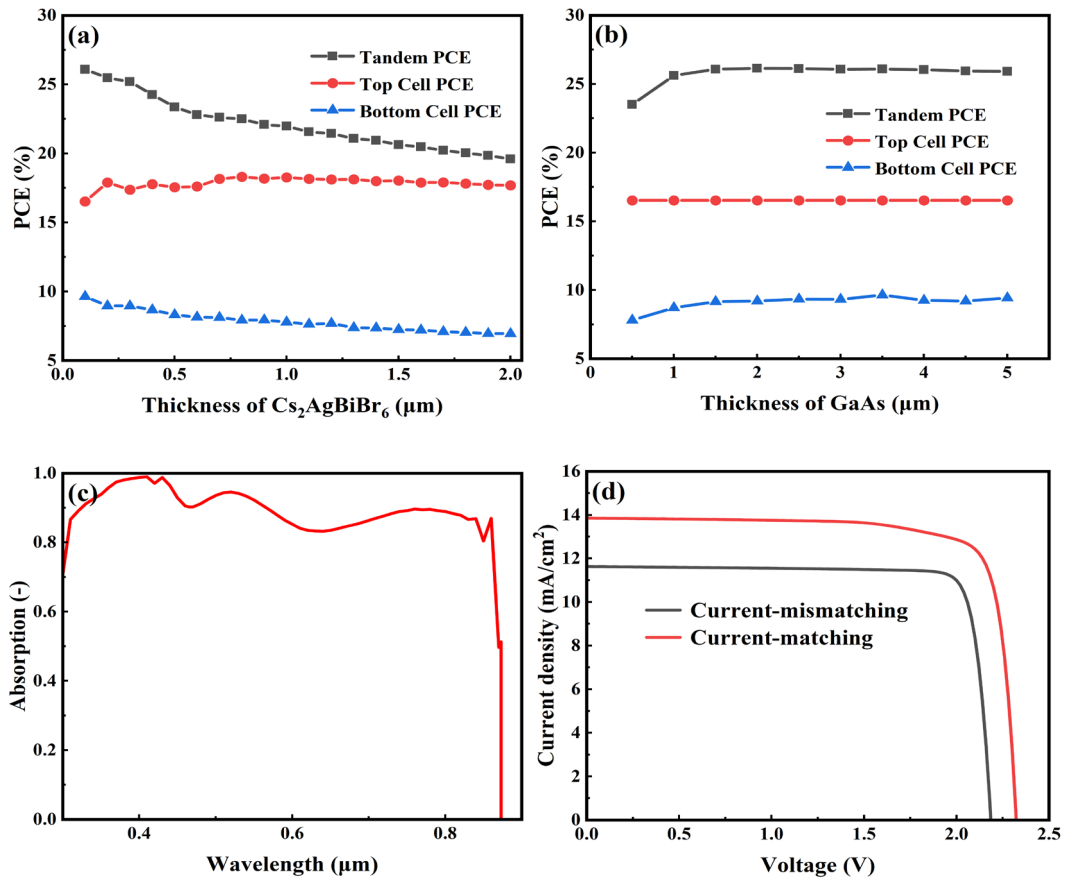


Fig. 8. 2-T tandem devices (a) variation of performance of subcells and tandem devices with the thickness of $\text{Cs}_2\text{AgBiBr}_6$, (b) variation of performance of subcells and tandem devices with the thickness of gallium arsenide substrate, (c) device light absorption rate and (d) 2-T tandem device performance under current mismatch and current matching.

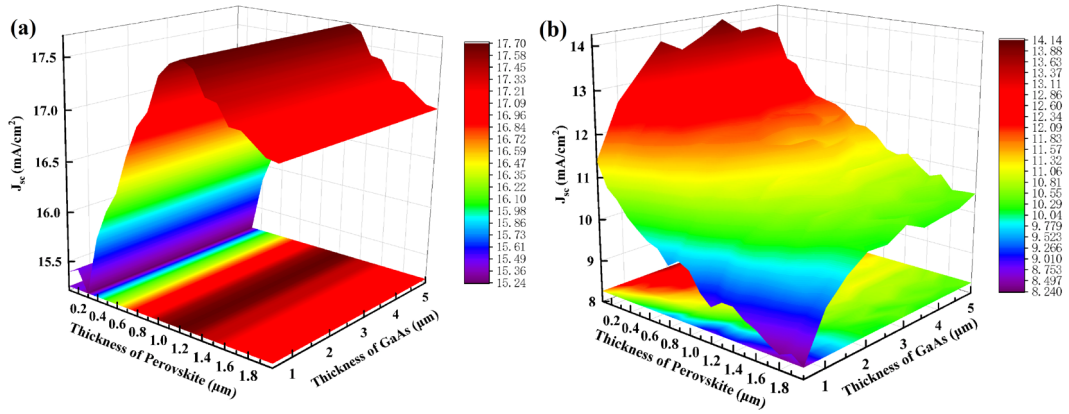


Fig. 9. Variation of subcells J_{sc} with the thickness of the light-absorbing layer in the subcells at spectral AM1.5G (a) $\text{Cs}_2\text{AgBiBr}_6$ solar cell (b) GaAs solar cell.

Consequently, the current balance point between the two subcells concerning current matching was determined through a simulation study of varying thicknesses of the $\text{Cs}_2\text{AgBiBr}_6$ and gallium arsenide substrate in this paper. The outcomes are illustrated in Fig. 9. The figure illustrates that when the thickness of the $\text{Cs}_2\text{AgBiBr}_6$ is $0.1 \mu\text{m}$, the thickness of the GaAs substrate is about $3.5 \mu\text{m}$, the currents between the subcells are the closest, the current loss is the smallest, and the device can obtain a higher photovoltaic conversion efficiency. According to the simulation results, the selection of the $\text{Cs}_2\text{AgBiBr}_6$ as the top cell, the lead-free double $\text{Cs}_2\text{AgBiBr}_6/\text{GaAs}$ tandem solar cell can obtain the optimal photoelectric conversion efficiency of 26.35%. The current matching J - V curve is depicted in Fig. 8(d); concurrently, the photon absorption rate of the 2-T $\text{Cs}_2\text{AgBiBr}_6/\text{gallium arsenide}$ tandem device is illustrated in Fig. 8(c).

To explore the influence of the doping concentration of the GaAs substrate on the efficiency of two-terminal tandem devices, this paper simulates the performance of the tandem device under various GaAs substrate layer doping concentrations; the results are illustrated in Fig. 10(d). The findings demonstrate that the overall performance of the tandem device initially rises and then declines with increasing doping concentration. Moreover, the J_{sc} of the two-terminal tandem device declined while the V_{oc} enhanced; this aligns with the results of the prior investigation regarding the doping concentration of the GaAs substrate layer of the four-terminal tandem device. The device achieves its optimal conversion efficiency when the doping concentration is 10^{17} cm^{-3} .

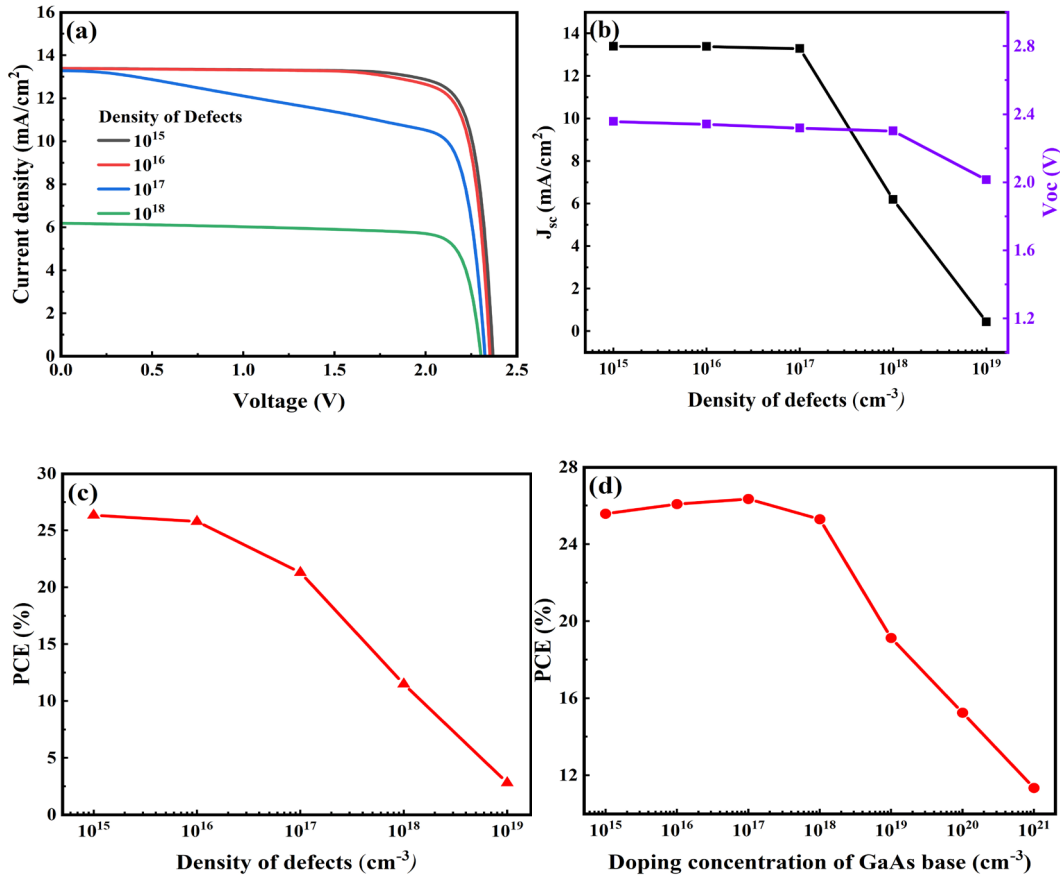


Fig. 10. (a), (b), (c) J-V curves, current and voltage, and photoelectric conversion efficiencies of the two-terminal tandem devices under different perovskite defect densities, respectively, and (d) photoelectric conversion efficiencies of the two-terminal Cs₂AgBiBr₆/gallium arsenide tandem devices under different GaAs substrate doping concentrations.

The defect density of perovskite films substantially influences the efficiency of tandem devices in the experiments [52]. This work initially establishes the defect density of Cs₂AgBiBr₆ at 10¹⁵ cm⁻³ and examines its impact on the performance of the two-terminal Cs₂AgBiBr₆/GaAs tandem device by altering the defect density. This paper simulates the impact of different defect densities of Cs₂AgBiBr₆ on the two-terminal Cs₂AgBiBr₆/GaAs tandem devices. The outcomes are shown in Figs 10(a)-(c), where an increase of defects significantly decreases the J_{sc} of the two-terminal Cs₂AgBiBr₆/GaAs tandem device, the V_{oc} of the device also shows a decreasing trend. When the defect density of the Cs₂AgBiBr₆ film is increased from 10¹⁵ cm⁻³ to 10¹⁹ cm⁻³, the V_{oc} of the two-terminal Cs₂AgBiBr₆/GaAs tandem device is reduced from 2.35V to 2.01V. The J_{sc} is reduced from 13.39 mA/cm² to 0.43 mA/cm², which makes the photoelectric conversion efficiency from 26.35% to 2.82%, indicating that the Cs₂AgBiBr₆ defect density substantially influences the efficiency of the two-terminal Cs₂AgBiBr₆/GaAs tandem device. The process should be enhanced as much as possible in the experiments to prepare high-quality lead-free Cs₂AgBiBr₆ thin films to reduce the loss of device performance.

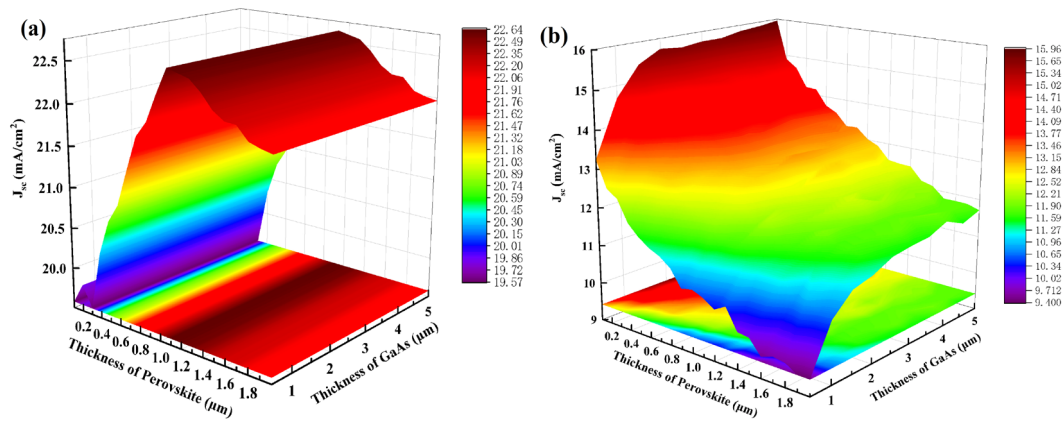


Fig. 11. Variation of subcells J_{sc} with the thickness of the light-absorbing layer in top and bottom cells under spectral AM0 (a) $\text{Cs}_2\text{AgBiBr}_6$ solar cell (b) GaAs solar cell.

To evaluate the efficiency of conventional double-junction GaAs solar cells in high-altitude and space applications, conducting studies under AM0 spectral conditions (solar spectrum outside the atmosphere) is frequently necessary [53]. Consequently, this paper also examines two-terminal $\text{Cs}_2\text{AgBiBr}_6/\text{GaAs}$ tandem devices in the context of AM0 spectra. The simulation outcomes indicate that the J_{sc} of the two-terminal $\text{Cs}_2\text{AgBiBr}_6/\text{GaAs}$ tandem device rises from 13.40 mA/cm² to 15.97 mA/cm². At the same time, the photoelectric conversion efficiency declines from 26.35% to 23.4% under the AM1.5G spectral condition, as illustrated in Fig. 12(b). Consequently, the photocurrent generated by light absorption in the device increases accordingly. Nevertheless, the device's photoelectric conversion efficiency decreases under the AM0 spectrum. The reason for this is that, on the one hand, due to the AM0 compared to AM1.5G, light irradiation intensity in the device absorption limit also has a tremendous increase in the part that can not be absorbed caused by the energy loss. On the other hand, as illustrated in Fig. 12(a), the increased irradiation intensity in the absorption range of the $\text{Cs}_2\text{AgBiBr}_6$ is significantly higher than that of the GaAs substrate. This leads to a more severe current mismatch in the AM0 spectrum and decreased device performance.

The current matching point remains constant under the AM0 spectrum, as illustrated in Fig. 11. Nevertheless, the two-terminal $\text{Cs}_2\text{AgBiBr}_6/\text{GaAs}$ tandem device performance is considerably impacted by the fact that the $\text{Cs}_2\text{AgBiBr}_6$ cell J_{sc} is significantly much greater than that of the GaAs cell in this spectrum, leading to a more severe current mismatch. The two-terminal $\text{Cs}_2\text{AgBiBr}_6/\text{GaAs}$ tandem device exhibits an efficiency of 23.40% under the AM0 spectrum. Additionally, the 2-T lead-free double $\text{Cs}_2\text{AgBiBr}_6/\text{GaAs}$ tandem solar cells have a certain degree of competitiveness and significant potential in high altitude and space applications because the fabrication cost is lower and the tunnelling junctions are simpler.

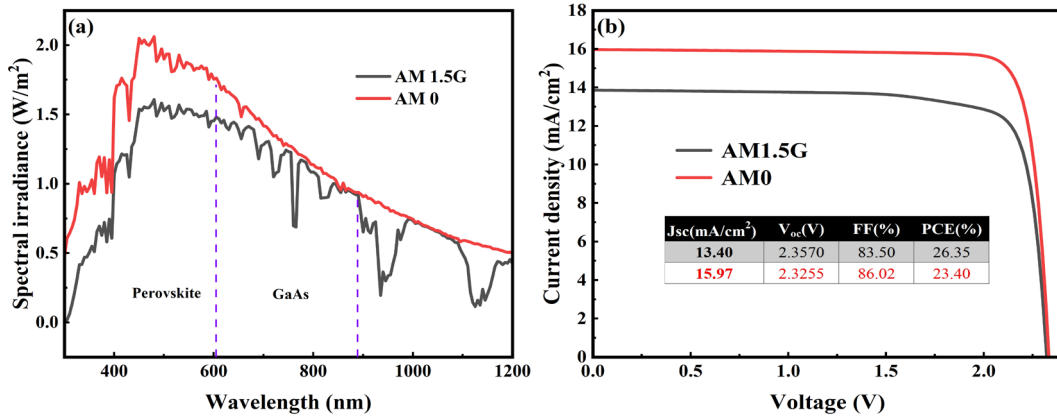


Fig. 12. (a). AM1.5G and AM0 spectra corresponding to the absorption of Cs₂AgBiBr₆ and gallium arsenide, and (b) J-V curves of the optimal two-terminal Cs₂AgBiBr₆/GaAs tandem device for AM1.5G and AM0 spectra.

4. Conclusion

This research presents a simulation analysis of 2-T and 4-T lead-free double Cs₂AgBiBr₆/gallium arsenide tandem solar cells featuring a planar structure. For the four-terminal Cs₂AgBiBr₆/gallium arsenide tandem device, the thicknesses of Cs₂AgBiBr₆, the carrier transport layer, and the gallium arsenide substrate are optimised to reduce the reflective losses and parasitic absorptions. Meanwhile, LiF material is applied to the top of the device to enhance light absorption and achieve high-performance tandem devices, and the top ITO layer is investigated. In addition, J_{sc} and V_{oc} tradeoffs are needed for high-efficiency GaAs cells; the optimal doping concentration of the GaAs substrate layer is 10^{17} cm^{-3} . For two-terminal tandem devices, current matching was performed, and the influence of the doping concentration of the GaAs substrate layer on the device efficiency was explored. The influence of Cs₂AgBiBr₆ defect density on the 2-T Cs₂AgBiBr₆/gallium arsenide tandem device was examined, and the results indicated that the Cs₂AgBiBr₆ defect density should be minimised to improve the device's performance. Finally, the performance of two-terminal Cs₂AgBiBr₆/gallium arsenide tandem devices under the AM0 spectrum was investigated, current matching was performed, and the 2-T Cs₂AgBiBr₆/gallium arsenide tandem device with a conversion efficiency of 23.40% was finally obtained.

Acknowledgements

This work was supported by the National Natural Science Foundation of China (No. 11964018) and the Natural Science Foundation of Jiangxi Province of China (Grant No. 20224BAB202032).

References

- [1] J. Burschka, N. Pellet, S. J. Moon, R. Humphry-Baker, P. Gao, M.K. Nazeeruddin, M. Grätzel, *Nature* 499, 316 (2013); <https://doi.org/10.1038/nature12340>
- [2] S. D. Stranks, G. E. Eperon, G. Grancini, C. Menelaou, M. J. P. Alcocer, T. Leijtens, L. M. Herz, A. Petrozza, H. J. Snaith, *Science* 342, 341 (2013); <https://doi.org/10.1126/science.1243>
- [3] Q. Zeng, X. Zhang, X. Feng, S. Lu, Z. Chen, X. Yong, S. A. T. Redfern, H. Wei, H. Wang, H. Shen, W. Zhang, W. Zheng, H. Zhang, J. S. Tse, B. Yang, *Advanced Materials* 30, 1705393 (2018); <https://doi.org/10.1002/adma.201705393>
- [4] B. Zhang, J. Su, X. Guo, L. Zhou, Z. Lin, L. Feng, J. Zhang, J. Chang, Y. Hao, *Advanced Science* 7, 1903044 (2020); <https://doi.org/10.1002/advs.201903044>
- [5] J. Chang, H. Zhu, B. Li, F. H. Isikgor, Y. Hao, Q. Xu, J. Ouyang, *Journal of Materials Chemistry A* 4, 887 (2016); <https://doi.org/10.1039/C5TA08398B>
- [6] J. Chang, Z. Lin, H. Zhu, F. H. Isikgor, Q. Xu, C. Zhang, Y. Hao, J. Ouyang, *Journal of Materials Chemistry A* 4, 16546 (2016); <https://doi.org/10.1039/C6TA06851K>
- [7] M. A. Green, E. D. Dunlop, M. Yoshita, N. Kopidakis, K. Bothe, G. Siefer, D. Hinken, M. Rauer, J. Hohl-Ebinger, X. Hao, *Progress in Photovoltaics: Research and Applications* 32, 425 (2024); <https://doi.org/10.1002/ppp.3831>
- [8] J. P. Correa-Baena, M. Saliba, T. Buonassisi, M. Grätzel, A. Abate, W. Tress, A. Hagfeldt, *Science* 358, 739 (2017); <https://doi.org/10.1126/science.aam6323>
- [9] L. Gao, I. Spanopoulos, W. Ke, S. Huang, I. Hadar, L. Chen, X. Li, G. Yang, M. G. Kanatzidis, *ACS Energy Letters* 4, 1763 (2019); <https://doi.org/10.1021/acsenergylett.9b00930>
- [10] S. Tang, Y. Deng, X. Zheng, Y. Bai, Y. Fang, Q. Dong, H. Wei, J. Huang, *Advanced Energy Materials* 7, 1700302 (2017); <https://doi.org/10.1002/aenm.201700302>
- [11] P. Li, W. Gao, C. Ran, H. Dong, X. Hou, Z. Wu, *Physica Status Solidi (a)* 216, 1900567 (2019); <https://doi.org/10.1002/pssa.201900567>
- [12] G. Volonakis, A. A. Haghighirad, R. L. Milot, W. H. Sio, M. R. Filip, B. Wenger, M. B. Johnston, L. M. Herz, H. J. Snaith, F. Giustino, *The Journal of Physical Chemistry Letters* 8, 772 (2017); <https://doi.org/10.1021/acs.jpcclett.6b02682>
- [13] S. E. Creutz, E. N. Crites, M. C. D. Siena, D. R. Gamelin, *Nano Letters* 18, 1118 (2018); <https://doi.org/10.1021/acs.nanolett.7b04659>
- [14] E. T. McClure, M. R. Ball, W. Windl, P. M. Woodward, *Chemistry of Materials* 28, 1348 (2016); <https://doi.org/10.1021/acs.chemmater.5b04231>
- [15] H. C. Sansom, G. Longo, A. D. Wright, L. R. V. Buizza, S. Mahesh, B. Wenger, M. Zanella, M. Abdi-Jalebi, M. J. Pitcher, M. S. Dyer, T. D. Manning, R. H. Friend, L. M. Herz, H. J. Snaith, J. B. Claridge, M. J. Rosseinsky, *Journal of the American Chemical Society* 143, 3983 (2021); <https://doi.org/10.1021/jacs.1c00495>
- [16] V. K. Ravi, N. Singhal, A. Nag, *Journal of Materials Chemistry A* 6, 21666 (2018); <https://doi.org/10.1039/C8TA06126B>
- [17] Z. Hu, Z. Lin, J. Su, J. Zhang, J. Chang, Y. Hao, *Solar RRL* 3, 1900304 (2019); <https://doi.org/10.1002/solr.201900304>
- [18] M. Bacha, A. Saadoune, I. Youcef, *Optical Materials* 131, 112671 (2022); <https://doi.org/10.1016/j.optmat.2022.112671>
- [19] K. O. Brinkmann, P. Wang, F. Lang, W. Li, X. Guo, F. Zimmermann, S. Olthof, D. Neher, Y.

- Hou, M. Stolterfoht, T. Wang, A. B. Djurišić, T. Riedl, *Nature Reviews Materials* 9, 202 (2024); <https://doi.org/10.1038/s41578-023-00642-1>
- [20] Z. Fang, Q. Zeng, C. Zuo, L. Zhang, H. Xiao, M. Cheng, F. Hao, Q. Bao, L. Zhang, Y. Yuan, W. Wu, D. Zhao, Y. Cheng, H. Tan, Z. Xiao, S. Yang, F. Liu, Z. Jin, J. Yan, L. Ding, *Science Bulletin* 66, 621 (2021); <https://doi.org/10.1016/j.scib.2020.11.006>
- [21] Z. Zhang, Z. Li, L. Meng, S. Y. Lien, P. Gao, *Advanced Functional Materials* 30, 2001904 (2020); <https://doi.org/10.1002/adfm.202001904>
- [22] C. D. Bailie, M. G. Christoforo, J. P. Mailoa, A. R. Bowring, E. L. Unger, W. H. Nguyen, J. Burschka, N. Pellet, J. Z. Lee, M. Grätzel, R. Noufi, T. Buonassisi, A. Salleo, M. D. McGehee, *Energy & Environmental Science* 8, 956 (2015); <https://doi.org/10.1039/C4EE03322A>
- [23] Q. Han, Y. T. Hsieh, L. Meng, J. L. Wu, P. Sun, E. P. Yao, S. Y. Chang, S. H. Bae, T. Kato, V. Bermudez, Y. Yang, *Science* 361, 904 (2018); <https://doi.org/10.1126/science.aat50>
- [24] Q. Zeng, L. Liu, Z. Xiao, F. Liu, Y. Hua, Y. Yuan, L. Ding, *Science Bulletin* 64, 885 (2019); <https://doi.org/10.1016/j.scib.2019.05.015>
- [25] D. P. McMeekin, G. Sadoughi, W. Rehman, G. E. Eperon, M. Saliba, M. T. Hörantner, A. Haghighirad, N. Sakai, L. Korte, B. Rech, M. B. Johnston, L. M. Herz, H. J. Snaith, *Science* 351, 151 (2016); <https://doi.org/10.1126/science.aad5845>
- [26] P. Löper, S. J. Moon, S. M. Nicolas, B. Niesen, M. Ledinsky, S. Nicolay, J. Bailat, J. H. Yum, S. D. Wolf, C. Ballif, *Physical Chemistry Chemical Physics* 17, 1619 (2015); <https://doi.org/10.1039/C4CP03788J>
- [27] J. H. Heo, S. H. Im, *Advanced Materials* 28, 5121 (2015); <https://doi.org/10.1002/adma.201501629>
- [28] Z. Li, T. H. Kim, S. Y. Han, Y. J. Yun, S. Jeong, B. Jo, S. A. Ok, W. Yim, S. H. Lee, K. Kim, S. Moon, J. Park, T. K. Ahn, H. Shin, J. Lee, H. J. Park, *Advanced Energy Materials* 10, 1903085 (2020); <https://doi.org/10.1002/aenm.201903085>
- [29] S. R. Kurtz, P. Faine, J. M. Olson, *Journal of Applied Physics* 68, 1890 (1990); <https://doi.org/10.1063/1.347177>
- [30] I. Cardinaletti, T. Vangerven, S. Nagels, R. Cornelissen, D. Schreurs, J. Hruby, J. Vodnik, D. Devisscher, J. Kesters, J. D'Haen, A. Franquet, V. Spampinato, T. Conard, W. Maes, W. Deferme, J. V. Manca, *Solar Energy Materials and Solar Cells* 182, 121 (2018); <https://doi.org/10.1016/j.solmat.2018.03.024>
- [31] M. Zhai, C. Chen, M. Cheng, *Solar Energy* 253, 563 (2023); <https://doi.org/10.1016/j.solener.2023.02.027>
- [32] P. K. Kung, M. H. Li, P. Y. Lin, J. Y. Jhang, M. Pantaler, D. C. Lupascu, G. Grancini, P. Chen, *Solar RRL* 4, 1900306 (2020); <https://doi.org/10.1002/solr.201900306>
- [33] G. Getachew, A. Wibrianto, A. S. Rasal, S. Kizhepat, W. B. Dirersa, V. Gurav, J. Y. Chang, *Progress in Materials Science*, 101192 (2023); <https://doi.org/10.1016/j.pmatsci.2023.101192>
- [34] H. Lei, D. Hardy, F. Gao, *Advanced Functional Materials* 31, 2105898 (2021); <https://doi.org/10.1002/adfm.202105898>
- [35] M. Yue, J. Su, P. Zhao, Z. Lin, J. Zhang, J. Chang, Y. Hao, *Nano-Micro Letters* 11, 1 (2019); <https://doi.org/10.1007/s40820-019-0320-y>
- [36] P. Zhao, J. Su, Z. Lin, J. Wang, J. Zhang, Y. Hao, X. Ouyang, J. Chang, *Materials Today Energy* 17, 100481 (2020); <https://doi.org/10.1016/j.mtener.2020.100481>
- [37] Silvaco, 2016 Atlas User's Guide [DB] Santa Clara USA

- [38] M. Hermle, G. Letay, S. P. Philipps, A. W. Bett, *Progress in Photovoltaics: Research and Applications* 16, 409 (2008); <https://doi.org/10.1002/pip.824>
- [39] K. A. Bertness, S. R. Kurtz, D. J. Friedman, A. E. Kibbler, C. Kramer, J. M. Olson, *Applied Physics Letters* 65, 989 (1994); <https://doi.org/10.1063/1.112171>
- [40] H. J. Jöbsis, V. M. Caselli, S. H. C. Askes, E. C. Garnett, T. J. Savenije, F. T. Rabouw, E. M. Hutter, *Applied Physics Letters* 119, 13 (2021); <https://doi.org/10.1063/5.0061899>
- [41] C. Stelling, C. R. Singh, M. Karg, T. A. F. König, M. Thelakkat, M. Retsch, *Scientific Reports* 7, 42530 (2017); <https://doi.org/10.1038/srep42530>
- [42] O. Aguilar, S. Castro, M. P. F. Godoy, M. R. S. Dias, *Optical Materials Express* 9, 3638 (2019); <https://doi.org/10.1364/OME.9.003638>
- [43] M. Schubert, V. Gottschalch, C. M. Herzinger, H. Yao, P. G. Snyder, J. A. Woollam, *Journal of Applied Physics* 77, 3416 (1995); <https://doi.org/10.1063/1.358632>
- [44] A. Minenkov, S. Hollweger, J. Duchoslav, O. Erdene-Ochir, M. Weise, E. Ermilova, A. Hertwig, M. Schiek, *ACS Applied Materials & Interfaces* 16, 9517 (2024); <https://doi.org/10.1021/acsmi.3c17923>
- [45] D. E. Aspnes, A. A. Studna, *Physical Review B* 27, 985 (1983); <https://doi.org/10.1103/PhysRevB.27.985>
- [46] Y. Wang, H. Tian, D. Zhang, W. Liu, X. Ma, J. Wang, *Journal of Electronic Materials* 52, 7728 (2023); <https://doi.org/10.1007/s11664-023-10692-4>
- [47] S. C. Yadav, J. A. K. Satrughna, P. M. Shirage, *Journal of Physics and Chemistry of Solids* 181, 111515 (2023); <https://doi.org/10.1016/j.jpcs.2023.111515>
- [48] I. Chabri, Y. Benhouria, A. Oubelkacem, A. Kaiba, I. Essaoudi, A. Ainane, *Optik* 274, 170560 (2023); <https://doi.org/10.1016/j.ijleo.2023.170560>
- [49] S. Rai, B. K. Pandey, A. Garg, D. K. Dwivedi, *Optical Materials* 121, 111645 (2021); <https://doi.org/10.1016/j.optmat.2021.111645>
- [50] I. Alam, R. Mollick, M. A. Ashraf, *Physica B: Condensed Matter* 618, 413187 (2021); <https://doi.org/10.1016/j.physb.2021.413187>
- [51] F. Z. Kharchich, A. Khamlichi, *Optik* 272, 170196 (2023); <https://doi.org/10.1016/j.ijleo.2022.170196>
- [52] T. S. Sherkar, C. Momblona, L. Gil-Escrig, J. Avila, M. Sessolo, H. J. Bolink, L. J. A. Koster, *ACS Energy Letters* 2, 1214 (2017); <https://doi.org/10.1021/acseenergylett.7b00236>
- [53] T. Takamoto, E. Ikeda, H. Kurita, M. Ohmori, *Applied Physics Letters* 70, 381 (1997); <https://doi.org/10.1063/1.118419>